21st Australasian Fluid Mechanics Conference
Adelaide, Australia
10-13 December 2018

Characteristics of passive scalar within Kármán vortices

J. G. Chen[1−2], R. A. Antonia[3], Y. Zhou[1−2] and T. M. Zhou[4]

[1]Institute for Turbulence-Noise-Vibration Interactions and Control
Harbin Institute of Technology (Shenzhen), Shenzhen 518055, China

[2]Digital Engineering Laboratory of Offshore Equipment, Shenzhen 518055, China

[3]School of Engineering, University of Newcastle, NSW 2308, Australia

[4]School of Civil, Environmental and Mining Engineering
The University of Western Australia, Crawley, WA 6009, Australia

Abstract

This work focuses on the statistical properties of the temperature (passive scalar) field exclusively inside the Kármán vortex based on the phase-averaging data, which are intrinsically different from the conventionally averaged statistics that weight all regions of the flow equally. The vortices are generated by a circular cylinder, and the fluctuating flow velocity and temperature behind the cylinder are simultaneously measured in the plane of mean shear at $x/d = 10$ where x is the streamwise distance from the cylinder centre and d is the cylinder diameter. The Reynolds number based on d and the free-stream velocity is 2.5×10^3. Statistics of the temperature fluctuation θ and its streamwise derivative $\theta_{,1}$, including their probability density function, skewness and kurtosis inside the Kármán vortex are found to follow a Gaussian distribution, which is distinctly different from their conventional counterparts. Both the conditional correlation coefficient between θ and $\theta_{,1}^2$ and the conditional expectation of $\theta_{,1}^2$ indicate that the temperature field inside the Kármán vortex is free from the effect of the large-scale events outside the vortex, like the cold/warm temperature front along the diverging separatrix and the coherent strain in the saddle region, so that the small- and large-scale fluctuating temperatures inside the vortex are at best weakly coupled, which is the major reason for the almost Gaussian behavior of the statistics of the temperature field inside the Kármán vortex.

Introduction

A distinct characteristic of a passive scalar such as heat mixed by a turbulent flow is the presence of the ramp-cliff structure in the temporal trace of the temperature fluctuation as a result of the temperature jump in the flow field [12]. This essentially reflects the fact that the temperature field is physically arranged in the form of concentration 'plateaus' separated by warm/cold temperature fronts [10]. Although the fronts are large-scale events, of the same order of magnitude as the integral scale, there is ample evidence that the ramp-cliff structures make an important contribution to the non-zero skewness of the temperature derivatives both in the streamwise and lateral directions [9, 11]. Warhaft [12] argued that it is this coupling between large- and small-scale characteristics which is at the origin of the departure from local isotropy of passive scalars in turbulent flows.

Antonia et al. [1] studied the topology of the velocity and temperature fields in the nearly self-preserving region of a turbulent plane jet and found that the temperature front is aligned with the diverging separatrix which connects adjacent vortical structures. A similar feature was also observed in the near/intermediate wake of a circular cylinder [2], where the diverging separatrix connects consecutive strong Kármán vortices of opposite sign. The study[2] also demonstrated that high temperature concentration occurs within the Kármán vortices when heat is injected into the flow via the boundary layer around the heated cylinder. Mi & Antonia [3] found that the temperature and voritcity fluctuaitons in the vortex display similar distribution. Husssain & Hayakawa [5] pointed out that the turbulence produced in the saddle region is transported along the diverging separatrix and accumulated in the region near the center of the Kármán vortex. Consequently, the Kármán vortices are also associated with the concentrations of the major incoherent random motions. Now that the temperature field within the vortex is spatially separated from the large-scale temperature front as well as from the coherent strain rate in the saddle region, one may expect that the large- and small-scale fluctuating temperatures within the Kármán vortex are statistically independent, and thus the temperature field within the Kármán vortex exhibits different statistical properties from those outside. However, it has not yet been confirmed in available literature. This is of fundamental importance. A positive answer may indicate that the passive scalar 'patch' around the core of the Kármán vortex (remote from the vortex boundary) would satisfy the local homogeneity and local isotropy reasonably well and thus allow the properties of the small-scale passive scalar to be examined, which is the major motivation of the present study.

Experimental details

A detailed description of the experimental configuration was given in [2] and here we briefly recall some important features of the experimental details. The experiment was conducted in an open-loop wind tunnel with a working section of 1.2 m (width) $\times$ 0.8 m (height) and 2.0 m long. A circular cylinder was used to generate the wake, which is a smooth brass tube of 110 cm long with an outer diameter d = 12.7 mm. A coiled heating wire was inserted into a ceramic tube, which was placed inside the cylinder to act as a heating element. A simplified sketch of the coordinate system, including symbol definitions, is shown in figure 1a. The free-stream velocity U_1 was 3.0 m/s, corresponding to a Reynolds number Re ($\equiv U_1 d/\nu$) of 2.5×10^3, where ν is the kinematic viscosity of air. A movable probe consisting of four X hot wires (X1 – X4 in figure 1b) and four cold wires (C1 – C4 in figure 1b) was used to capture the velocity and temperature fluctuations as well as their spatial derivatives simultaneously. Measurements were conducted within the cylinder mid-span plane at x^* = 10, 20 and 40. Hereafter, an asterisk denotes normalization by d for convenience.

The focus is primarily on the statistics of the temperature fluctuation θ and its streamwise derivative $\theta_{,1}$ ($\equiv \partial\theta/\partial x$) at $x^* = 10$. The unheated cylinder wake is assumed to be statistically symmetrical about the centerline. As a result, the present measurements were made only on one side of the centerline, i.e., y^* =

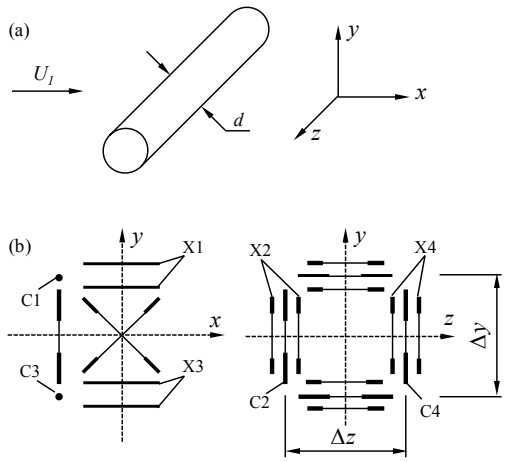

Figure 1: Simplified sketch of the coordinate system and the definitions of symbols.

-0.2 to 2.8, with a transverse measurement increment of about 0.2. The maximum mean temperature excess $\overline{\Theta}_0$ on the centerline, with respect to the ambient fluid, is about 1.6°C, which is small enough to avoid any buoyancy effects, and hence allows the heat to be treated as a passive scalar.

The streamwise $\theta_{,1}$ is estimated using Taylor's hypothesis, i.e., $\theta_{,1} \approx \Delta\theta/(-\Delta t U_c)$ where $U_c = 0.87U_1$ is average convection velocity of the vortices and $\Delta\theta$ is the difference between the consecutive points in the time series of the temperature fluctuation and $\Delta t = 1/f_{samp}$, where f_{samp} = 2500 Hz is the sampling frequency. The sampling period of time is about 45s. Note that [7] valiedated the use of Taylor's hypothesis in the near wake of a circular cylinder for a Reynolds number similar to that in the present experiment. The spatial resolution of the measurement in the x direction is estimated to be about 5.8η where $\eta \equiv (\nu^3/\overline{\varepsilon})^{1/4}$ is the Kolmogorov length scale on the wake centerline and $\overline{\varepsilon}$ is approximated by assuming transverse (y-z plane) homogeneity, instead of isotropy.

Results and discussion

For a clear visualization of the temperature field, the isocontours of the phase-averaged temperature fluctuation in [2] are replotted here in figure 2a. The detailed description of the phase-average technique is provided in [2]. Phase averaging is based on a total of 1980 detected vortex shedding periods so that the coherent component $\widetilde{\theta}$ of θ may be extracted, as shown in figure 2a, with the random fluctuation of θ removed. The phase ϕ can be interpreted in terms of a longitudinal distance based on Taylor's hypothesis, and ϕ = 0 - 2π corresponds to the vortex wavelength. The Kármán vortex centers and saddle points, identified from the phase-averaged sectional streamlines (not shown), are marked by '+' and '×', respectively. The thick dashed lines give an approximate idea of the vortex boundary. The inclined dash-dotted line passing through the saddle point represents the diverging separatrix.

Figure 2a clearly shows that the warm fluid (positive $\widetilde{\theta}$) is distributed concentrically within the Kármán vortices, while the cold fluid (negative $\widetilde{\theta}$) entrained by the vortices from the ambient free stream resides in the alley way between consecutive vortices. A large-scale warm/cold temperature front forms approximately along the diverging separatrix, which is in accord with Antonia et al.'s [1] observation in a plane jet. Figure 2b displays the probability density function (pdf) of the temperature relative to the ambient temperature $P_{\Theta(\phi=0)}(\Theta \equiv \theta + \overline{\Theta}$,

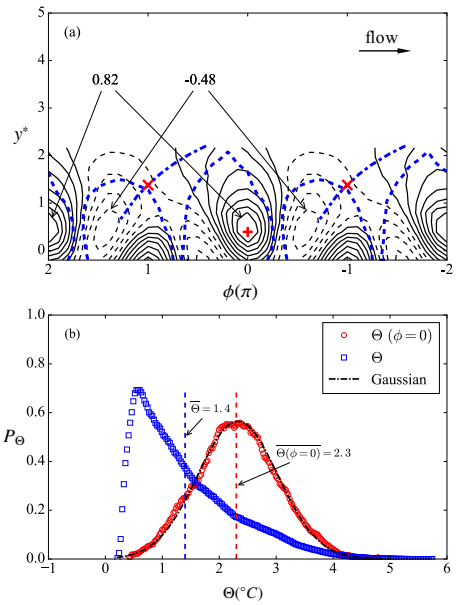

Figure 2: (a) Isocontours of phase-averaged temperature $\widetilde{\theta}$. Flow is from left to right, as indicated by the horizontal arrow. (b) Probability density function of $\Theta(\phi = 0)$ and Θ (relative to the ambient temperature) at $y^* = y_c^*$. The Gaussian distribution with the same mean and standard deviation as the pdf of $\Theta(\phi = 0)$ is also shown.

where $\overline{\Theta}$ is the mean temperature relative to the ambient) at the vortex center, that is, the conditional pdf of Θ given $\phi = 0$ at $y^* = y_c^*$ where $y_c^* = 0.39$ is the lateral position of the vortex center (figure 2a). The conventional pdf, P_Θ, of Θ at the same lateral position is also presented for comparison. Interestingly, $P_{\Theta(\phi=0)}$ follows a Gaussian distribution almost perfectly, while P_Θ displays a relatively sharp cutoff on its left side because of the presence of the cold fluid. Note that the cutoff temperature of P_Θ is very close to the ambient temperature, i.e. 0 (the temperature in figure 2 is relative to the ambient temperature). The characteristic of the nearly Gaussian temperature distribution is further confirmed by the skewness (S) and kurtosis (K) of θ at other locations within the vortex (figure 3). The skewness $S_{\theta(\phi=0)}$ of the temperature fluctuation across the vortex (y^* = 0 - 1.4, ϕ = 0), is closer to 0 than the conventional S_θ, particularly at the position corresponding to the vortex center ($y^* = y_c^*$). The larger positive S_θ reflects the presence of the long positive tail of P_Θ in figure 2b. A similar observation applies when comparing the kurtosis of the temperature within the vortex $K_{\theta(\phi=0)}$ with the conventional K_θ across the Kámán vortex (figure 3b); $K_{\theta(\phi=0)}$ is in general closer to the Gaussian value of 3 than K_θ.

The large-scale temperature front is always associated with a large temperature gradient, thus resulting in the non-Gaussian statistics of the temperature field [4]. The practically Gaussian distribution of temperature within the vortex is consistent with the observation that only warm fluid appears about the vortex center (figure 2a), and indicates that the temperature field near the center of the vortex is free of large temperature jump.

The pdf, $P_{\theta,1(\phi=0)}$, of $\theta_{,1}$ at the Kámán vortex center, i.e. the conditional pdf of $\theta_{,1}$ given $\phi = 0$ at $y^* = y_c^*$, is compared in figure 4 with the conventional pdf, $P_{\theta_{,1}}$, of $\theta_{,1}$ at the same lateral position ($y^* = y_c^*$). The log-linear scale is used in order to highlight the tails of the pdf. As expected, $P_{\theta_{,1}}$ departs significantly from the Gaussian distribution, displaying exponential tails, which is consistent with the previous observations [12].

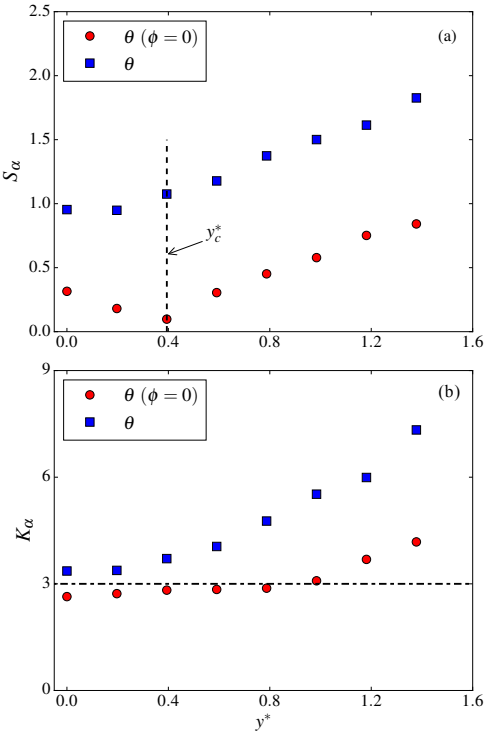

Figure 3: Lateral distribution of (a) skewness and (b) kurtosis of $\theta(\phi = 0)$ and θ. The vertical dashed line in (a) marks the lateral position corresponding to the vortex center. The horizontal dashed-line in (b) marks the value of 3, the kurtosis of a Gaussian distribution.

Interestingly, $P_{\theta,1(\phi=0)}$ tends to have only slightly broader tails compared with the Gaussian distribution. The difference between $P_{\theta,1}$ and $P_{\theta,1(\phi=0)}$ highlights the distinct statistical properties of the small-scale temperature within and outside the Kámán vortex. This is also confirmed by the difference between the skewnesses $S_{\theta,1}$ and $S_{\theta,1(\phi=0)}$ or the kurtosises $K_{\theta,1}$ and $K_{\theta,1(\phi=0)}$, as shown in figure 5. Compared to $S_{\theta,1}$, $S_{\theta,1(\phi=0)}$ is closer to 0 at locations above the vortex center ($y^* > 0.4$), especially at $y^* = 0.6 - 1.0$ (figure 5a). It is noted that the magnitude of $S_{\theta,1(\phi=0)}$ is increasing as y^* approaches the wake centerline. This is because as y^* decreases to 0, it gets closer to the vortex periphery where the temperature gradient becomes larger compared to that in the vortex core region. Similarly, $K_{\theta,1(\phi=0)}$ is closer in magnitude to the Gaussian value of 3 than $K_{\theta,1}$ at the same lateral position (figure 5b).

Filled with random incoherent motions [5], the vortex roll acts to form, within its boundary, a high concentration of small-scale temperature fluctuations of warm fluid, while the large-scale temperature front occurs outside the vortex along the diverging separatrix [1, 2]. We use $\theta_{,1}^2$, which is one component of the temperature variance dissipation rate $\overline{\chi}$ ($\equiv \kappa(\overline{\theta_{,1}^2} + \overline{\theta_{,y}^2} + \overline{\theta_{,z}^2})$; κ is the thermal diffusivity), to characterize the small-scale temperature. The conditional correlation coefficient, i.e. the correlation coefficient between θ and $\theta_{,1}^2$ with the same ϕ (at the same y^* position), is defined as

$$\rho(\theta, \theta_{,1}^2 | \phi) \equiv \left[\frac{\overline{(\theta - \overline{\theta})(\theta_{,1}^2 - \overline{\theta_{,1}^2})}}{\sigma_\theta \sigma_{\theta_{,1}^2}} | \phi \right] \qquad (1)$$

where σ is the standard deviation of a fluctuating variable. Figure 6a shows the color-filled isocontours of $\rho(\theta, \theta_{,1}^2 | \phi)$, superposed onto the isocontours of the phase-averaged temperature (shown in figure 2a), the latter serving as a reference. A large value of $\rho(\theta, \theta_{,1}^2 | \phi)$, about 0.5, appears in the saddle region along the diverging separatrix where the large-scale temperature front forms, while small values, about 0.05 (i.e. one order of magnitude smaller), can be found in the downstream half of the vortex. The minimum correlation coefficient is displaced from the vortex center, probably because of the physical separation between concentrations of θ and $\theta_{,1}^2$ within the vortex. One may expect that the dependence between θ and $\theta_{,1}^2$ is weak in a region where the correlation coefficient is small so that (small-scale) $\theta_{,1}^2$ is statistically independent of (large-scale) θ. To characterize the dependence of $\theta_{,1}^2$ on θ, the conditional expectation (or mean value) of $\theta_{,1}^2(\phi)$, i.e. $E(\theta_{,1}^2(\phi)|\theta(\phi))^\dagger$, is examined in figure 6b, where '†' denotes normalization by $\overline{\theta_{,1}^2(\phi)}$. Phases ϕ = 0, -0.1π, -0.2π and ϕ = -0.8π correspond to the locations, in figure 6a, where $\rho(\theta, \theta_{,1}^2 | \phi)$ is small and large, respectively. A constant $E(\theta_{,1}^2(\phi)|\theta(\phi))^\dagger$ is expected when $\theta_{,1}^2(\phi)$ and $\theta(\phi)$ are statistically independent of each other. For locations associated with a small correlation coefficient, $E(\theta_{,1}^2(\phi)|\theta(\phi))^\dagger$ is generally equal to unity, indicating that $\theta_{,1}^2(\phi)$ is statistically independent of $\theta(\phi)$. In contrast, $E(\theta_{,1}^2(\phi)|\theta(\phi))^\dagger$ shows a dependence on $\theta(\phi)$ when the correlation coefficient is large. A large value of $E(\theta_{,1}^2(\phi)|\theta(\phi))^\dagger$ is generally associated with a large magnitude of $\theta(\phi)$, except when $\theta(\phi)/\theta(\phi)_{rms}$ is extremely large.

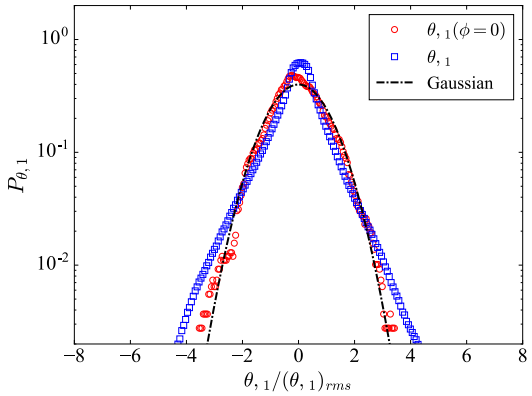

Figure 4: Probability density function of $\theta_{,1}(\phi = 0)$ and $\theta_{,1}$ at $y^* = y_c^*$.

The results of figure 6 provide some useful physical insight into the difference between the phase-averaged and conventional statistics of the temperature field. Along the diverging separatrix in the saddle region where the large-scale temperature front presents, the small-scale temperature fluctuations are significantly affected by the large scales, as reflected by the large correlation coefficient between θ and $\theta_{,1}^2$ in the saddle region (figure 6a) and the appreciable dependence of $E(\theta_{,1}^2(\phi)|\theta(\phi))^\dagger$ on $\theta(\phi)$ for ϕ = -0.8π (figure 6b). Previous studies have shown that this coupling between large and small scales is responsible for the non-Gaussian statistics of the temperature field [6, 11]. The coherent strain in the saddle region may play a role in the interaction between the large and small temperature scales since the strain rate may act to amplify the temperature gradient [8]. Conversely, the temperature field within the Kámán vortex is 'isolated' by the vortex structure from the effect of the large-scale temperature front as well as the coherent strain in the saddle region. As such, the small-scale temperature fluctuations are only weakly affected by the large-scales, as evidenced by the small value of $\rho(\theta, \theta_{,1}^2 | \phi)$ within the vortex (figure 6a) and

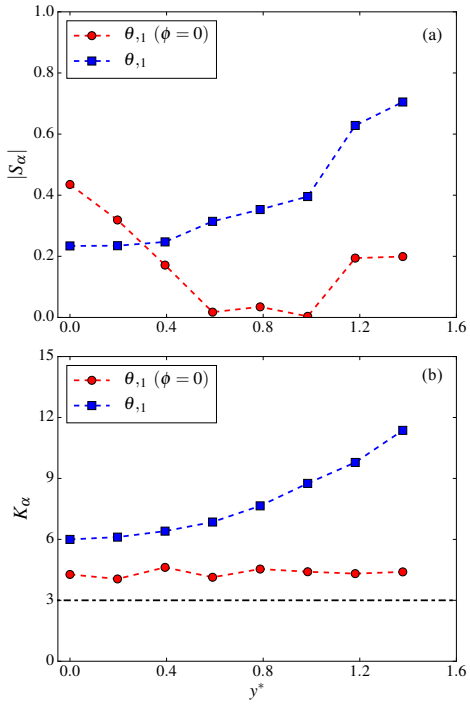

Figure 5: Lateral distribution of the (a) absolute value of skewness and (b) kurtosis of $\theta_{,1}\ (\phi = 0)$ and $\theta_{,1}$. The horizontal dashed-line in (b) marks the value of 3, the kurtosis of a Gaussian distribution.

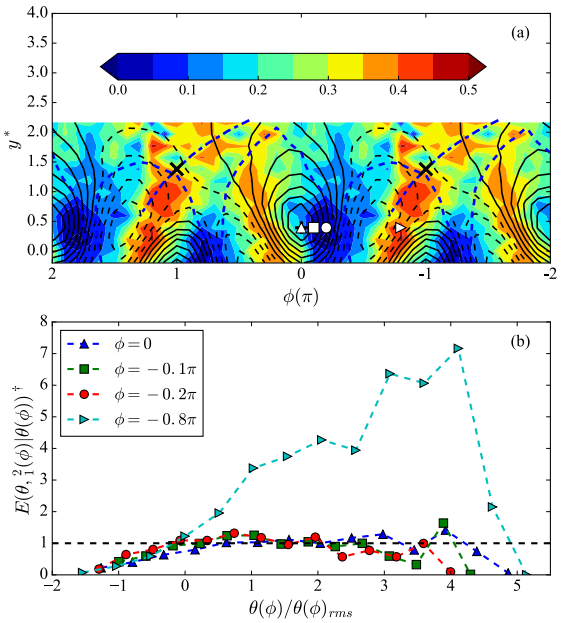

Figure 6: (a) Color-filled isocontours of the correlation coefficient between θ and $\theta_{,1}^2$ at the same phase, superposed with the isocontours of $\widetilde{\theta}$. The four values of ϕ in (b) correspond to the phases of the four markers indicated in (a).

the almost constancy of $E(\theta_{,1}^2(\phi)|\theta(\phi))^\dagger$ for $\phi = 0$ to -0.2π (figure 6b). The incoherent random motions within the vortex lead to the nearly Gaussian behaviors of both θ and $\theta_{,1}$ in this region.

Conclusions

The temperature field in the Kármán vortex displays quite different statistical features from the corresponding conventional statistics. The vortex structure acts to segregate the temperature field inside Kármán vortices from the large-scale temperature front in the saddle region. Consequently, the small- and large-scale temperature fluctuations inside the vortex are at most weakly coupled. Despite the relatively small Taylor micro-scale Reynolds number (about 100), the nearly zero skewness of the temperature derivative within the Kármán vortex suggests that the associated temperature field is much closer to local isotropy than that outside.

Acknowledgments

YZ wishes to acknowledge support given to him from NSFC through grants 11632006 and U1613226 and from Research Grants Council of Shenzhen Government through grants JCYJ20160531193220561 and JCY20160531192108351.

References

[1] Antonia, R.A., Chambers, A.J., Britz, D., Browne, L., Organized structures in a turbulent plane jet: topology and contribution to momentum and heat transport. *J. Fluid Mech.*, **172**, 1986, 211–229.

[2] Chen, J.G., Zhou, Y., Zhou, T.M., Antonia, R.A., Three-dimensional vorticity, momentum and heat transport in a turbulent cylinder wake. *J. Fluid Mech.*, **809**, 2016, 135–167.

[3] Mi, J., Antonia, R. A. Temperature distribution within vortices in the wake of a cylinder. *Int. J. Heat Mass Transfer.* **37**, 1994, 1048–1050.

[4] Gollub, J.P., Clarke, J., Gharib, M., Lane, B., Mesquita, O.N., Fluctuations and transport in a stirred fluid with a mean gradient. *Phys. Rev. Lett.* **67**, 1991, 3507–3510.

[5] Hussain, A.K.M.F., Hayakawa, M., Eduction of large-scale organized structures in a turbulent plane wake. *J. Fluid Mech.*, **180**, 1987, 193–229.

[6] Jayesh, Warhaft, Z., Probability distribution, conditional dissipation, and transport of passive temperature fluctuations in gridgenerated turbulence. *Phys. Fluids A* **4**, 1992, 2292-2307.

[7] Mi, J., Antonia, R.A., Approach to local axisymmetry in a turbulent cylinder wake. *Exp. Fluids*, **48**, 2010, 933–947.

[8] Pumir, A., A numerical study of the mixing of a passive scalar in three dimensions in the presence of a mean gradient. *Phys. Fluids*, **6**, 1994, 2118-2132.

[9] Sreenivasan, K.R., Antonia, R.A., 1977. Skewness of temperature derivatives in turbulent shear flows. *Phys. Fluids*, **20**, 1977, 1986.

[10] Shraiman, B.I., Siggia, E.D., Scalar turbulence. *Nature*, **405**, 2000, 639–646.

[11] Tong, C., Warhaft, Z., On passive scalar derivative statistics in grid turbulence. *Phys. Fluids*, **6**, 1994, 2165–2176.

[12] Warhaft, Z., Passive scalars in turbulent flows. *Annu. Rev. Fluid Mech.*, **32**, 2000, 203–240.